Direct experimental access to microscopic dynamics in liquid hydrogen

M. Celli, D. Colognesi, and M. Zoppi
Consiglio Nazionale delle Ricerche, Istituto di Fisica Applicata "Nello Carrara," Via Panciatichi 56/30, 50127 Firenze, Italy
(Received 12 March 2002; published 12 August 2002)

We have obtained the double-differential incoherent neutron scattering cross section of liquid and solid parahydrogen in various thermodynamic conditions using TOSCA, a time-of-flight, inverse geometry, crystal analyzer spectrometer, operating at the pulsed neutron source ISIS. The measured cross section provides direct experimental access to the self part of the center-of-mass inelastic structure factor of the parahydrogen molecules in the system. Data have been corrected for the experimental effects and then analyzed in the framework of the Young-Koppel model and the Gaussian approximation. The velocity autocorrelation functions and their energy spectra have been obtained from a fitting procedure, making use of the quantum generalized Langevin equation and of model memory functions, and finally compared to the most recent results of both molecular centroid dynamics and self-consistent quantum mode-coupling theory. Some dynamic quantities were also related to simple equilibrium properties and simulated through a standard path integral Monte Carlo code. Results are very interesting but still urge for further developments of theoretical and dynamic simulation approaches, as well as for more extensive experimental efforts.

DOI: 10.1103/PhysRevE.66.021202 PACS number(s): 61.20.−p, 61.12.Ex, 64.70.Dv

I. INTRODUCTION

In the recent years the microscopic dynamics of simple liquids has attracted many researchers with the consequent production of a large literature [1]. As far as classical simple liquids are concerned, this massive work has generated a wealth of experimental data that can be satisfactory interpreted within a well established theoretical framework [2]. In addition, in those cases where a purely theoretical approach becomes insufficient, one can rely on numerical methods (e.g., molecular dynamics computer simulation), which allow to obtain any time-dependent correlation function that is experimentally accessible [3]. On the other hand, for quantum and semiclassical liquids the situation is far less satisfactory: only approximate methods can be used and, when quantum effects begin to play a crucial role, a full theoretical calculation of the spectral features becomes quite difficult, if not totally impossible. It means that a rigorous description of the quantum dynamics in a simple fluid (especially for $T>0$) at the microscopic level is still an open problem in the physics of disordered systems. So far, no fully satisfactory theoretical approach has been proved to give a complete and precise description of the dynamics of a quantum liquid, and even computer simulation has not reached the necessary accuracy that is needed in order to give quantitatively acceptable predictions of the relevant dynamic quantities, with the only possible exception of ground-state superfluid ^{4}He [4].

On the experimental side, the inelastic neutron scattering technique [5] seems to have gained a prominent role as a source of reliable information on the dynamics of simple liquids [6]. As a matter of fact, the double-differential neutron scattering cross section, which was originally derived by Van Hove [7], is truly quantal. This has allowed an extensive experimental work on the dynamic properties of the helium liquids [8]. However, intrinsic experimental difficulties have prevented, so far, a complete experimental exploration of the dynamic properties of other simple quantum liquids (e.g., the hydrogens). Nowadays this field is becoming more and more accessible with the development of the last generation neutron sources and of novel instrumentation [9].

If we consider liquid ^{4}He, the idea goes immediately to its superfluid properties. This is a very peculiar case, where the structural and dynamical properties of the liquid are heavily affected by its quantum (Bose-Einstein) statistics. However, there are important cases where the exchange of particles does not play an appreciable role, but the structure and dynamics are still largely determined by the quantum delocalization properties [10]. This is the case of the normal phase of liquid ^{4}He, liquid ^{3}He at $T>T_F$(T_F is the Fermi temperature) and of the liquid hydrogens (H_2, D_2, and T_2). Liquid Ne exhibits visible quantum features too. However, in this case, the quantum effects are sufficiently small that a perturbative theoretical approach (e.g., the Wigner-Kirkwood expansion [11]) is usually sufficiently accurate to describe the observed structural and dynamic characteristics. Thus, when quantum effects play a relevant role, we can broadly distinguish between two main categories of liquids, as suggested for the first time by Dyugaev [10]: on one side we have liquid systems where the exchange of particles is relevant and Bose-Einstein (superfluid ^{4}He) or Fermi-Dirac (cold liquid ^{3}He at $T<T_F$) statistics should be applied; on the other side we have liquids, like the hydrogens, where the exchange is negligible (and the Boltzmann statistics satisfactorily applies), but the quantum delocalization effects are still relevant. In the latter case microscopic features are affected by quantum mechanical effects in a way that cannot be simply dealt with through a perturbative approach.

In recent years computer simulation has been of great help in interpreting the features of the liquid state at the microscopic level. As far as static properties are concerned, Monte Carlo (MC) methods [3,12] are routinely used to predict the microscopic structure of liquids, once a suitable interaction potential is provided [13]. In turn, dynamic features can be evaluated using the molecular dynamics technique [14–17]. Unfortunately, these two simulation procedures apply to classical liquids only. When quantum fluids are in-

volved, both simulation methods break down. However, as far as the static structure is concerned, the path integral Monte Carlo (PIMC) simulation technique has been developed [18–20], allowing to determine the microscopic equilibrium properties of quantum liquids and solids, even at the level of the superfluid phase of ^{4}He [21,22]. The PIMC simulation technique is based on a factorization of the density matrix [23,24]: the quantum system is replaced by a system of classical ring polymers, which may be simulated using classical MC. Each ring polymer consists of P copies of the quantum particle (P being the Trotter number [25]) and exact quantum mechanical results are obtained in the limit $P \to \infty$. It is important to point out that a rigorous isomorphism between the quantum system and the set of classical ring polymers has been established and explained by Chandler and Wolynes [26]. On the contrary, the state of the art of the simulation techniques dealing with the dynamics of quantum liquids is not yet established on a firm and rigorous basis, even though some very interesting results have begun to appear in the literature [27–33], especially from the so-called path integral centroid molecular dynamics approach. In this context we should also distinguish among the various ranges of magnitude of the momentum transfer, $\hbar k$. In the very low k region, where the hydrodynamic approximations can be still applied, the dynamic behavior of a quantum system is generally understood (at least at a semiquantitative level) and only quantitative refinements are necessary [34]. At the other end of the k scale, when the impulse approximation (IA) applies, the dynamic behavior of quantum liquids is also well described: the energy ($\hbar\omega$) and momentum transfers are so large that the interparticle interactions during the scattering process can be almost neglected, or accounted for by using small final state effect corrections [8]. In this case, the only important microscopic features that determine the neutron scattering law are the molecule recoil energy and the single-particle momentum distribution of molecular centers of mass [35]. In the IA the most prominent effect of the interactions resides, before the scattering process, in a quantum renormalization of the translational kinetic energy which (at low temperature) becomes strongly density dependent [36,37]. Thus the dynamic problem is virtually solved in the two extreme scenarios: where the quantum system can be considered either as a uniform continuous (very low values of k, as the ones probed by optical spectroscopy) or as a set of almost freely recoiling particles (very high values of k and ω, as in deep inelastic neutron scattering).

It is in the region of intermediate k that the dynamical problem is still partially unsolved from the theoretical point of view, at least as far as quantum and semiquantum fluids are concerned. This is the range of k where the static structure factor $S(k)$ shows its main features and the microscopic quantum dynamics of the system is heavily determined by the interaction of each molecule with its neighbors. Preliminary attempts to shed some light on this topic have been historically carried out by Vineyard [38], who introduced some important approximations in the theoretical evaluation of the dynamic structure factor $S(k,\omega)$. The theory has been later developed, in the framework of the well-known fluctuation-dissipation theorem, by Rahman, Singwi, and Sjölander in an important work appeared in 1962 [39], and further extensions and approximations have been subsequently proposed by Nelkin and Ghatak [40], Zwanzig [41], and Sears [42]. More recently, a self-consistent quantum mode-coupling (QMC) theory has been suggested by Rabani and Reichman [43] and applied to the case of liquid parahydrogen. This model starts from a definition of an *exact* quantum generalized Langevin equation which follows from the historical works of Zwanzig [44], Mori [45,46], and Kubo [47]. Using static structural information from PIMC simulations, a simple quantum viscoelastic model (suggested by Lovesey [48]), and a pure exponential decay law for the time dependence of the memory function, the authors [43] have been able to obtain a satisfactory result for the dynamic structure factor of liquid parahydrogen at $T=14$ K. However, no direct quantitative comparison with the available experimental results [49,50] was provided [43].

From the computational point of view, one could implement a brute-force method, like the one invented to simulate the Newtonian dynamics of a large (but finite) number of classical particles. However, in this case, one should simultaneously solve the Schrödinger equation for all the molecules in the interaction field generated by their neighbors. Obviously this is an extremely hard task, even taking into account the present capability of the fastest supercomputers. Alternatively, one has to rely on approximate simulation methods that are appearing in literature and look quite promising for evaluating the dynamic features of quantum systems [32]. Presently, the comparison with the *dynamic* experimental results is fairly good, at least to a semiquantitative level [50]. In this context, any precise experimental dynamic information comparable to theoretical or simulation predictions is extremely valuable.

In this paper, we present the results of an experiment on liquid parahydrogen that satisfies some of the above mentioned requirements. On one side, the measured spectral results are sufficiently precise to allow a fine quantitative comparison with the available theoretical and simulation predictions. On the other hand, the span of momentum transfer is considerably larger than the extent to which hydrodynamics applies. Actually, the present experimental results provide direct information on the single particle molecular dynamics in rather interesting momentum and energy transfer ranges. The experimental scattering law, related to the self inelastic structure factor $S_{self}(k,\omega)$ extends from $\hbar\omega = -10$ meV up to $\hbar\omega = 80$ meV, while the momentum transfer, $\hbar k$, monotonically grows from 3 Å^{-1} to 8 Å^{-1}. Thus, due to the relatively high value of k, the purely diffusive motion is not the main issue in our spectra and we expect that only approximate information on the self-diffusion coefficient D will be worked out. However, owing to the extended energy variation, we will be able to obtain reliable information on other dynamic quantities, as well as on the time correlation functions of some selected observable. In Sec. II we will recollect the relevant theoretical framework of our study and we will discuss the approximations used in the present work. The experiment will be described in Sec. III, and we will show how to determine directly the self (incoherent) inelastic dynamic structure factor of liquid

parahydrogen from the experimental spectra. In Sec. IV we will explain how to obtain the velocity autocorrelation function and its spectral shape by using the Gaussian approximation for the intermediate scattering function. Finally, in Sec. V, we will discuss the results and we will compare the quantities derived from the experimental spectra with their estimates obtained from literature and from PIMC simulations.

II. THEORETICAL FRAMEWORK

Following Van Hove [7], we define the intermediate scattering function for the molecular centers of mass, $F(\mathbf{k},t)$, as

$$F(\mathbf{k},t)=\frac{1}{N}\sum_{j,l}\langle\exp[-i\mathbf{k}\cdot\mathbf{r}_j(0)]\exp[i\mathbf{k}\cdot\mathbf{r}_l(t)]\rangle, \quad (1)$$

where $\hbar\mathbf{k}$ is the momentum transfer, $\mathbf{r}_l(t)$ represents the Heisenberg operator for the center-of-mass position of molecule l at time t, and $\langle\cdots\rangle$ indicates a quantum statistical average. As we are interested in the single molecule dynamics, we need only to deal with the *self* part of the intermediate scattering function, which is

$$F_{self}(\mathbf{k},t)=\frac{1}{N}\sum_{j}\langle\exp[-i\mathbf{k}\cdot\mathbf{r}_j(0)]\exp[i\mathbf{k}\cdot\mathbf{r}_j(t)]\rangle$$
$$=\langle\exp[-i\mathbf{k}\cdot\mathbf{r}_1(0)]\exp[i\mathbf{k}\cdot\mathbf{r}_1(t)]\rangle. \quad (2)$$

The calculation of $F_{self}(\mathbf{k},t)$ is not a trivial task, especially in a quantum liquid. However, Rahman *et al.* [39] have shown that it can be rigorously written in an isotropic system as

$$F(k,t)=\exp\left(it\frac{\hbar k^2}{2M}\right)\exp\left[\sum_{n=1}^{\infty}(-k^2)^n\gamma_n(t)\right], \quad (3)$$

where M is the molecular mass. The first exponential represents the recoil energy term and the functions $\gamma_n(t)$ are expressed by means of the quantum statistical averages of the velocity operators. We note that Eq. (3) is rigorous, while limiting the cumulant expansion to the first term represents the well-known Gaussian approximation [38]. In this case, all the dynamic information is contained in $\gamma_1(t)$, given by

$$\gamma_1(t)=\int_0^t dt_1\int_0^{t_1}dt_2\langle v_k(t_2)v_k(t_1)\rangle, \quad (4)$$

where $v_k=(\mathbf{v}\cdot\mathbf{k})/k$ is the projection of the velocity $\mathbf{v}$ along the $\mathbf{k}$ direction. Taking into account the translational time invariance of the quantum statistical average, Eq. (4) becomes

$$\gamma_1(t)=\int_0^t dt_1(t-t_1)\langle v_k(0)v_k(t_1)\rangle. \quad (5)$$

This can be written, for an isotropic system, as

$$\gamma_1(t)=\frac{1}{3}\int_0^t dt_1(t-t_1)u(t), \quad (6)$$

which directly connects the function $\gamma_1(t)$ to the velocity autocorrelation function (VACF) $u(t)$ defined as

$$u(t)=\langle\mathbf{v}(0)\cdot\mathbf{v}(t)\rangle. \quad (7)$$

The next two terms in the cumulant expansion appearing in Eq. (3), i.e., $\gamma_2(t)$ and $\gamma_3(t)$, are given explicitly by Rahman *et al.* [39]. These functions are determined by the irreducible correlation functions among four and six velocities, respectively.

Within the applicability limit of the Gaussian approximation, the velocity correlation function determines uniquely the self intermediate scattering function and, consequently, the self dynamic structure factor. Now we define the power spectrum of the VACF, $J(\omega)$, by means of the Fourier transform

$$J(\omega)=\frac{1}{2\pi}\int_{-\infty}^{+\infty}dte^{-i\omega t}u(t). \quad (8)$$

In a quantum system, because of the intrinsic structure of $u(t)$, some constraints apply to the power spectrum $J(\omega)$ [5,51]. For example, from the property $u(-t)=u^{\star}(t)$, it follows that $J(\omega)$ is real, while from the property $u(-t)=u(t+i\beta\hbar)$, where $\beta=1/(k_BT)$ and k_B is the Boltzmann constant, the well-known detailed balance condition follows:

$$J(-\omega)=\exp(-\beta\hbar\omega)J(\omega). \quad (9)$$

If we split the power spectrum $J(\omega)$ in its symmetric and antisymmetric components, i.e., we define

$$J(\omega)=J_S(\omega)+J_A(\omega), \quad (10)$$

where

$$J_S(\omega)=\frac{1}{2}[J(\omega)+J(-\omega)] \quad (11)$$

and

$$J_A(\omega)=\frac{1}{2}[J(\omega)-J(-\omega)], \quad (12)$$

it turns out that the symmetric component $J_S(\omega)$ is given by the real part of $u(t)$, while the imaginary part determines the antisymmetric term $J_A(\omega)$,

$$J_S(\omega)=\frac{1}{\pi}\int_0^{\infty}dt\cos(\omega t)\mathrm{Re}[u(t)], \quad (13)$$

$$J_A(\omega)=\frac{1}{\pi}\int_0^{\infty}dt\sin(\omega t)\mathrm{Im}[u(t)]. \quad (14)$$

Finally, using the detailed balance condition of Eq. (9), it is possible to relate the two spectra and to obtain

$$J_A(\omega)=\frac{1-e^{-\beta\hbar\omega}}{1+e^{-\beta\hbar\omega}}J_S(\omega)=\tanh(\beta\hbar\omega/2)J_S(\omega), \quad (15)$$

which is one of the many possible ways of expressing the aforementioned fluctuation-dissipation theorem. We observe that the two functions, $f(\omega)$ and $g(\omega)$, defined by Rahman *et al.* [39] and related to the energy spectra of the imaginary and the real parts of $u(t)$, are simply connected to the antisymmetric and symmetric components of $J(\omega)$ through

$$J_A(\omega)=\frac{3\hbar}{4M}\omega f(\omega), \tag{16}$$

$$J_S(\omega)=\frac{3k_BT}{2M}g(\omega). \tag{17}$$

From the zeroth moment of $J(\omega)$ one writes

$$\int_{-\infty}^{+\infty}d\omega J(\omega)=2\int_0^{\infty}d\omega J_S(\omega)=u(0)=\frac{\langle E_k\rangle}{M/2}, \tag{18}$$

where $\langle E_k\rangle$ is the single particle mean kinetic energy and the normalization condition for $g(\omega)$ follows:

$$\int_0^{\infty}d\omega g(\omega)=\frac{\langle E_k\rangle}{(3/2)\,k_BT}. \tag{19}$$

It is worth noting that the mean kinetic energy in a quantum system differs from the classical expression (namely, $\langle E_k^{cl}\rangle = 3/2k_BT$) and therefore the integral of $g(\omega)$ equals 1 only in the classical limit. Finally, still following Rahman *et al.* [39], it is easy to obtain the normalization condition for the function $f(\omega)$,

$$\int_0^{\infty}d\omega\quad f(\omega)=1. \tag{20}$$

Now we have all the ingredients to compute, given the VACF or its energy spectrum, the self-dynamic structure factor,

$$S_{self}(k,\omega)=\frac{1}{2\pi}\int_{-\infty}^{+\infty}dte^{-i\omega t}F_{self}(k,t), \tag{21}$$

which becomes, within the Gaussian approximation [i.e., Eq. (3) truncated at the first order],

$$S_{self}(k,\omega)\cong\frac{1}{\pi}\int_0^{\infty}dt\,\exp[-k^2\gamma_1^R(t)]\cos[(\omega-\omega_r)t + k^2\gamma_1^I(t)], \tag{22}$$

where $\omega_r=\hbar k^2/(2M)$ is the recoil frequency and $\gamma_1^R(t)$ and $\gamma_1^I(t)$ are the real and imaginary parts of the mean square displacement function $\gamma_1(t)$, respectively, as defined in Eq. (6). These two mean square displacement functions are easily obtained from the components of the spectrum $J(\omega)$,

$$\gamma_1^R(t)=\frac{2}{3}\int_0^{\infty}d\omega\,\frac{J_S(\omega)}{\omega^2}[1-\cos(\omega t)], \tag{23}$$

$$\gamma_1^I(t)=-\frac{2}{3}\int_0^{\infty}d\omega\,\frac{J_A(\omega)}{\omega^2}\sin(\omega t). \tag{24}$$

Within the applicability limit of the Gaussian approximation, the single particle dynamic problem reduces to find a reliable model for the VACF $u(t)$ [see Eq. (7)]. This is relatively simple in classical liquids, where a memory function approach can help in solving the problem [2]. The situation becomes more difficult in the quantum case where $u(t)$ is a complex function. However, it has been shown [27] that this difficulty can be circumvented taking advantage of the symmetry properties of the Kubo transform of the VACF. Following Kubo [52] we define a *canonical* velocity autocorrelation function $u^c(t)$ according to the prescription

$$u^c(t)=\frac{1}{\beta}\int_0^{\beta}d\lambda\langle e^{\lambda\mathcal{H}}\mathbf{v}(0)e^{-\lambda\mathcal{H}}\cdot\mathbf{v}(t)\rangle, \tag{25}$$

where $\mathcal{H}$ is the Hamiltonian of the system. This *canonical* VACF turns out to be even in time [52] and its Fourier transform reads

$$J^c(\omega)=\frac{1}{2\pi}\int_{-\infty}^{+\infty}dte^{-i\omega t}u^c(t). \tag{26}$$

This turns out to be simply related to the *symmetric* and *antisymmetric* spectra of $u(t)$ by

$$J^c(\omega)=\frac{\tanh(\beta\hbar\omega/2)}{(\beta\hbar\omega/2)}J_S(\omega), \tag{27}$$

$$J^c(\omega)=\frac{1}{(\beta\hbar\omega/2)}J_A(\omega). \tag{28}$$

Equations (25), (27), and (28) are also known as the *Kubo transforms* in time and frequency space, respectively.

III. EXPERIMENT DESCRIPTION

The neutron scattering experiment was carried out on TOSCA-I, a crystal-analyzer inverse-geometry spectrometer operating at the ISIS pulsed neutron source (Rutherford Appleton Laboratory, Chilton, Didcot, UK) [53]. The incident neutron beam spanned a broad energy (E_i) range and the energy selection was carried out on the secondary neutron flight path using the (002) Bragg reflection of ten graphite single crystals placed in backscattering around 136.6°. This fixed the nominal scattered neutron energy to $\simeq$3.5 meV. Higher order Bragg reflections were filtered out by 15 cm thick beryllium blocks cooled down to 30 K. This geometry allows to cover an extended energy transfer range, even though the fixed position of the crystal analyzers and the small value of the neutron final energy imply a variation in k which is a monotonic function of ω. The resolving power of TOSCA-I was rather good ($1.4\%<\Delta\hbar\omega/E_i<3.5\%$) in the energy transfer region relevant to the present experiment (4 meV$<\hbar\omega<$114 meV). The extended spectral range of TOSCA makes this instrument a sort of neutron equivalent of a Raman optical spectrometer.

Intramolecular transitions could be in principle easily observed well beyond the first vibrational transition of molecular hydrogen (we remind that this is placed at 514.5 meV). However, it should be also pointed out that, due to the molecular recoil, the observed shifts are generally much greater than those observed on a conventional Raman spectrometer. The Raman spectrum of liquid hydrogen is characterized by strong intramolecular transitions (rotations and vibrations). However, on the Stokes (energy-loss) side of each intramolecular line, a side phonon band of intermolecular origin is visible [54] and originates from the same mechanism that produces the broad quasielastic band that is attributed to collective multiphonon excitations. Similar concepts can be applied to the neutron scattering spectrum from liquid hydrogen. Here the fundamental difference between the quasielastic (no intramolecular excitation is involved) and the inelastic (one or more intramolecular excitations are involved) contributions is due to the different weight of the self and distinct translational components. Actually in the quasielastic spectrum, the Van Hove [7] formulation applies and the contribution to the neutron double-differential cross section is a mixing of the two components (self and distinct), as in any monatomic liquid. However, due to the lack of correlation among the phase factors in the intramolecular transitions pertaining to different molecules, only the self term builds up and contributes to the inelastic neutron spectrum.

Thus, TOSCA can be considered even more as the neutron equivalent of an optical Raman spectrometer, the only difference being the momentum transfer monotonically growing along with the energy shift: $k_{\omega\to\infty}\to(2m_n\omega/\hbar)^{1/2}$, where m_n is the neutron mass. In the high-energy region of the spectrum the momentum transfer grows to such an extent that the scattering process is expected to enter the IA regime. Therefore, the spectrum carries information relative to the momentum distribution of the centers of mass [55]. On the other hand, in the low energy spectral region, the size of the momentum transfer is of the order of the reciprocal of the intermolecular distances between neighbors. In this case the self contribution to the scattering function is expected to provide information on the dynamics, mainly driven by the pair interactions. Even though the transition between these two regimes is not clearly defined, it is sensible to assume [2] that it lies beyond the first peak of the intermolecular static structure factor $S(k)$ (which is located around $k=2$ Å^{-1}) in the region where $S(k)$ becomes $\simeq 1$ (i.e., $k\simeq 6$–8 Å^{-1}). Should the momentum transfer decrease to much lower values, to such an extent that the hydrodynamic regime would drive the microscopic dynamics, it would be possible to gain direct information on the long-time behavior of the VACF and the self-diffusion coefficient [6]. Unfortunately, this is not the case of TOSCA and only an approximate estimate of the diffusive dynamics is expected to come out from the present hydrogen spectra.

If pure liquid parahydrogen is considered, the inelastic neutron spectrum becomes rather simple (see Fig. 1). Due to the low experimental temperature ($T=14$–21 K) only the fundamental rotational state ($J=0$) is populated. In addition, since the transitions to the even states ($J=0\to J'=2,4,6,\ldots$) are weighted by the small hydrogen coherent cross-section ($\sigma_c=1.8$ b), their intensity is almost two orders of magnitude smaller than the transitions to the odd states (driven by the incoherent one, $\sigma_i=80$ b) [5]. Thus the observed spectrum reduces, for any practical purpose, to a set of odd rotational transitions ($J=0\to J'=1,3,5,\ldots$). Due to the small moment of inertia of hydrogen, rotational transitions are all well separated ($J=0\to J'=1$ implies an energy jump of 14.7 meV, while $J=0\to J'=3$ corresponds to a jump of 88.2 meV). As a consequence, taking into account the extra shift induced by the molecular recoil (see Fig. 2), the overlap of different bands is small and each band can be separately analyzed. The high-energy region of the spectra, involving the rotational transitions beyond the first excited rotational level, ($J=0\to J'=3,5,7$) has been already analyzed in the framework of the IA regime [55] (as shown

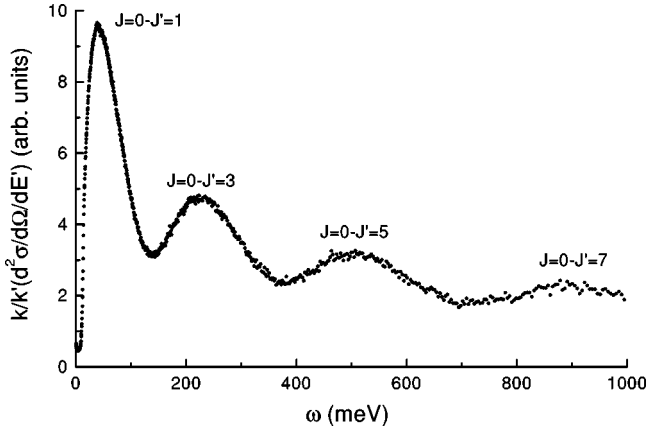

FIG. 1. Raw experimental inelastic neutron spectrum (after can subtraction) measured on liquid parahydrogen at $T=17.2$ K and $p=0.43$ bar. Each peak represents a rotational transition starting from the ground level $J=0$. The transition to the even levels are weighted by the small H coherent cross section, therefore only the transitions to the odd levels $J'=1,3,5,7$ are visible.

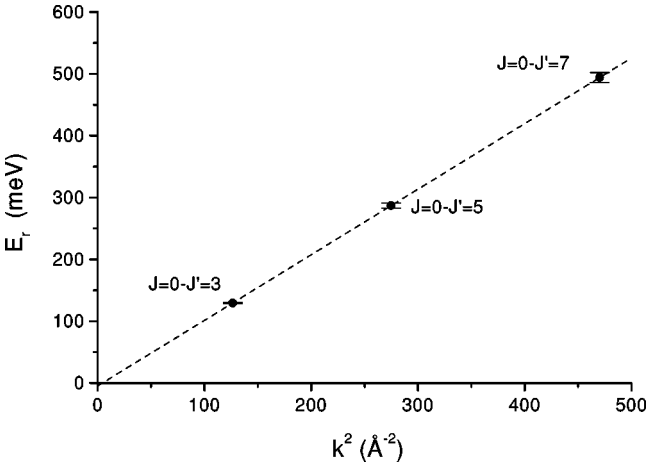

FIG. 2. Recoil energies, E_r, as a function of the square of the momentum transfer from the spectrum of liquid parahydrogen at $T=14.3$ K. The slope of the linear fit (dashed line) is proportional to the inverse of the recoil mass [55] which turns out to be $M=(1.99\pm 0.01)$ amu. This demonstrates that we observe the whole molecule recoil.

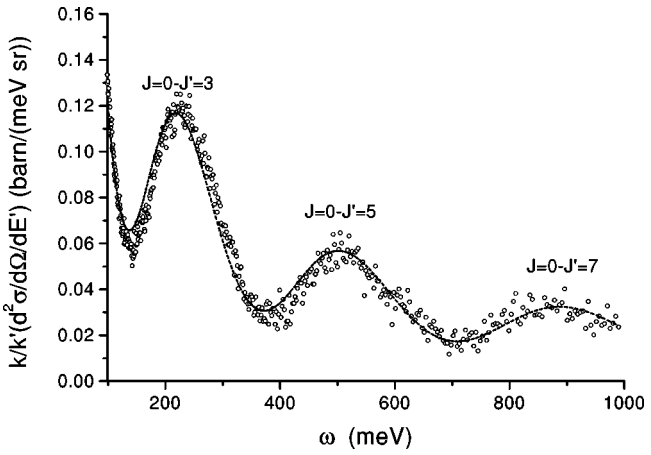

FIG. 3. Experimental inelastic spectrum measured on liquid parahydrogen at $T=14.3$ K after subtracting can contribution and multiple scattering. The $J=0\rightarrow J'=1$ transition is not reported in the picture because in this case the impulse approximation does not apply. The line represents the best fit to the data using the impulse approximation and a Gaussian function for the momentum distribution. From the fit we could extract [55] the center-of-mass (translational) mean kinetic energy, $\langle E_k \rangle$.

in Fig. 3). In this case, due to the high value of the momentum and energy transfers, the intermolecular interactions only give rise to a simple renormalization of the center-of-mass mean kinetic energy. This, in turn, affects the width of the molecular recoil peak which describes the free motion of the molecule. A simple modification of the Young-Koppel theory [56] can be applied and we could determine the translational mean kinetic energy in liquid and solid hydrogen as a function of the thermodynamic conditions [55].

If we focus our attention on the first rotational transition ($J=0\rightarrow J'=1$) of molecular parahydrogen, the double-differential cross section is given by [57]

$$\frac{d^2\sigma}{d\Omega d\omega}=\frac{k_1}{k_0}\frac{\sigma_i}{4\pi}|f(k)|^2_{0\rightarrow 1}S_{self}(k,\omega)\otimes\delta(\omega-\omega_{0\rightarrow 1}), \tag{29}$$

where $f(k)$ is the intramolecular form factor and $S_{self}(k,\omega)$ is the dynamic structure factor for the self motion of the molecular center of mass. The symbol $\otimes$ represents an energy convolution and δ is the Dirac delta function. In this case the value of the momentum transfer is not large enough ($k<8$ Å^{-1}) to justify the use of the IA and $S_{self}(k,\omega)$ carries much information on the effects of the intermolecular interactions on the single particle dynamics of molecular hydrogen. In order to establish a comparison with various simulations and theoretical models, due to the instrumental characteristics of TOSCA, the cross section in Eq. (29) should be evaluated along the kinematic path of the spectrometer, provided a suitable model is given for $S_{self}(k,\omega)$.

The measurement was carried out at seven thermodynamic points. Five were selected in the liquid phase (see Table I) and two in the solid one (see Ref. [55] for the description of the solid phase measurements and the high-energy data analysis). After performing the background measurements of the empty cryostat, we cooled the empty container at the desired temperature ($T=17.2$ K) and we measured its time-of-flight (TOF) neutron spectrum. Then hydrogen was allowed to condense in the scattering cell. This was made of aluminum (1.0 mm thick walls) with a circular-slab geometry. The sample thickness was also 1.0 mm and the cell diameter (50.0 mm) was slightly larger that the beam cross section. The pressure of the gas handling system was set to $p=0.43$ bar [slightly larger than the corresponding saturated vapor pressure (SVP)] in order to make sure that the cell was filled with liquid (the SVP at $T=17.2$ K is 0.36 bar). At the bottom of the scattering container, out of the neutron beam, we had inserted some powder of a paramagnetic catalyst made of Cr_2O_3 on an Al_2O_3 substrate in order to speed up the conversion from orthohydrogen to parahydrogen. The relative concentration of the two species was monitored looking at the scattering spectrum. In particular, we could observe the progressive disappearance of the $J=1\rightarrow J'=1$ (quasielastic line) transition, which is weighted by the incoherent cross-section of the proton [58], from the low energy portion of the spectrum. When this spectral feature was below the limit of detectability (in practice, masked by the $J=0\rightarrow J'=0$ transition, which is weighted by the coherent cross section of the proton) we assumed that the equilibrium had been reached. The equilibration process took, in our case, about 20–25 h. The estimated concentration of parahydrogen, based on the theoretical calculation [59], was assumed to be 99.96%. Then we started recording the scattering spectrum up to an integrated proton current of 2271 μA h (roughly, 12 h of beam time).

TABLE I. Thermodynamic conditions of the measured liquid hydrogen samples, including the theoretically calculated parahydrogen percentage [p-H_2] and integrated proton current IC. The triple point temperature is $T_{TP}=13.803$ K.

T (K)	n (nm^{-3})	p (bar)	[p-H_2] (%)	IC (μA h)
14.3(2)	22.91(6)	0.16(1)	99.99	2368
15.7(2)	22.52(6)	0.24(1)	99.98	1917
17.2(2)	22.10(6)	0.43(1)	99.96	2271
19.2(2)	21.50(6)	0.82(1)	99.88	2310
21.2(2)	20.83(9)	1.34(1)	99.71	1344

The following spectra were collected in a similar way, after changing the temperature and pressure of the sample, and performing some short test spectra, to make sure that the sample was already at the equilibrium composition. The stability of the thermodynamic conditions during the experiment was very good. Temperature fluctuations never exceeded 0.1 K and pressure fluctuations were of the same order of magnitude of the pressure gauge sensitivity (i.e., 0.01 bar). The temperature uncertainty estimated for our measurements (see Table I), i.e., 0.2 K, was mainly due to a tiny gradient across the vertical dimension of the sample cell. The densities of our samples (and their uncertainties) were later derived according to Ref. [59]. The full set of parameters characterizing the present experiment is reported in Table I. In Fig. 4(a) we show the raw spectrum of liquid parahydrogen at $T=14.3$ K and $n=22.91$ nm^{-3} in the re-

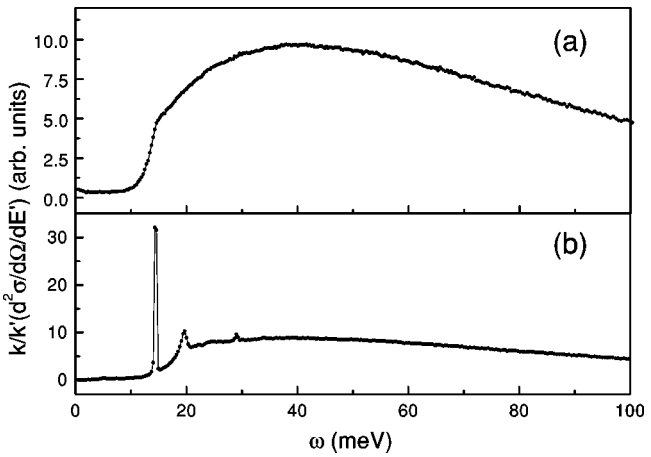

FIG. 4. (a) Raw experimental inelastic spectrum measured on liquid parahydrogen at $T=14.3$ K (after can subtraction) zoomed in the low-energy zone ($\hbar\omega<100$ meV). (b) Raw experimental inelastic spectrum measured on solid parahydrogen [55] at $T=12.2$ K and $n=26.02$ nm^{-3} (after can subtraction) zoomed in the same low-energy zone. The unrecoiled $J=0\rightarrow J'=1$ transition is evident at $\hbar\omega=14.42(3)$ meV.

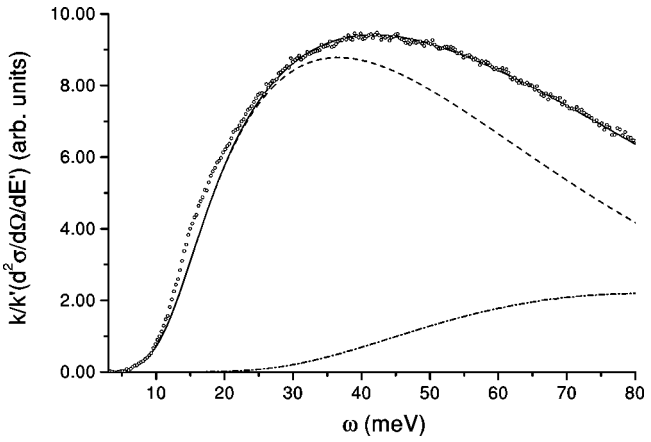

FIG. 5. Inelastic spectrum measured on liquid parahydrogen at $T=21.2$ K in the energy region of the $J=0\rightarrow J'=1$ transition (circles). Experimental data are compared to the simulated single-scattering (dashed line) and multiple-scattering (dot-dashed line) spectra and their sum (solid line). The multiple-scattering contribution is subsequently subtracted from the data.

gion of the first rotational transition ($J=0\rightarrow J'=1$). As a comparison the lower part, Fig. 4(b), shows the equivalent spectrum for the solid sample [55] at $T=12.2$ K and $n=26.02$ nm^{-3}. In the liquid phase, the rotational line ($J=0\rightarrow J'=1$) is broadened and shifted by a combination with the diffusive motion and the intermolecular excitations [60], while in the solid phase spectrum, a relevant fraction of the hydrogen molecules transfers the recoil to the whole lattice and an extremely sharp rotational line appears in the unshifted position of 14.42(3) meV.

IV. DATA ANALYSIS

The experimental TOF spectra were transformed into energy transfer data, detector by detector, making use of the standard TOSCA-I routines available on the spectrometer, and then added together exploiting the narrow angular range spanned by the whole set of detectors ($\Delta\theta=9.5°$) [53]. In this way, we produced a single double-differential cross-section measurement along the TOSCA-I kinematic path $[k(\omega),\omega]$ for each thermodynamic condition of Table I. Then, data were corrected for the k_1/k_0 factor and subtracted of the tiny empty can contribution, separately recorded at $T=17.2$ K (with an integrated proton current of 749 μA h). Two fundamental corrections were carefully performed: *multiple scattering* evaluation and *self-absorption* attenuation. As far as the former is concerned, we simulated both single-scattering and multiple-scattering neutron spectra measured by TOSCA-I for each sample through the analytical approach suggested by Agrawal in the case of an infinite flat slablike sample [61]. The main inputs of this procedure were the self inelastic structure factors of the samples to be measured in a wide region of the (k,ω) plane. These functions were simulated through the Gaussian approximation (already described in Sec. II and in Ref. [39]) using a model spectral function $f(\omega)$ [see Eq. (16)]. This simple heuristic model was already positively tested by the authors [62] for liquid parahydrogen in a large energy range. It assumes a Gaussian shape for $f(\omega)$, fixing its three parameters (amplitude, mean, and standard deviation) by imposing the overall normalization [see Eq. (20)] in the positive ω region, the value of the translational mean kinetic energy [39] and the self-diffusion coefficient [39]. The mean kinetic energy was obtained from Ref. [55] while the self-diffusion coefficient was derived from the experimental data of Ref. [63].

The two simulated spectra (single and multiple) were added together in the 4 meV$<\hbar\omega<$80 meV interval of TOSCA-I. Then the unknown instrumental constant was worked out and all the experimental data were subtracted of their respective multiple scattering contributions. An example of this procedure is shown in Fig. 5, where the agreement between experimental and simulated data at $T=21.2$ K is appreciable, considering the extreme simplicity of the model for $f(\omega)$. The only visible disagreement is in the low-energy region (10 meV$<\hbar\omega<$25 meV) where, however, the multiple scattering contribution appears to be negligible. As we will see in the following section, a more elaborated model for $f(\omega)$ can largely improve the agreement between experimental and simulated data.

Following this stage, self-absorption correction was applied to the normalized single-scattering experimental data, still assuming the infinite slab approximation and making use of the aforementioned analytical approach [61]. However, in this case, no model was employed for the parahydrogen total scattering cross section, which, on the contrary, was obtained from the experimental results of direct measurements on the SVP liquid p-H_2 at $T=16.0(2)$ K [64]. At the end of the correction procedure, the processed data, limited to the 4 meV$<\hbar\omega<$80 meV interval, were corrected for the rotational dynamics. Since, in this energy region, the $J=0\rightarrow J'=3,5,7$ transitions are negligible, the spectrum was divided by the intramolecular form factor for the $J=0\rightarrow J'=1$ transition [56] $j_1^2(kd/2)$, where d is the mean interatomic

distance in H_2 and $j_1(x)$ the spherical Bessel function of the first order. Then, an energy shift of $E_{0-1}=14.42$ meV, i.e., the pure $J=0\rightarrow J'=1$ transition energy derived from the present solid parahydrogen measurements, was applied to remove the effect of the δ function in Eq. (29).

From Eq. (29) and the knowledge of $k(\omega)$, we could extract the $S_{self}(k(\omega),\omega)$, i.e., the projection of the incoherent dynamic structure factor of condensed hydrogen on the kinematic path of TOSCA [53]. In order to compare the experimental data with the results of the calculations, we rely on the Gaussian approximation [39]. This is known to be rigorous in a harmonic solid but becomes less accurate in the case of a liquid, even in the classical case [2]. In particular, the approximation is known to be good in the low k region, where the dynamics is mainly driven by the hydrodynamic diffusive modes, and in the very high k region, where the IA for the dynamics of the molecular centers of mass can be applied. Actually, in this latter case, the Gaussian approximation becomes rigorous, also for the liquid state, provided the momentum distribution of a particle in the fluid, $n(\mathbf{p})$, is Gaussian. This is generally the case, even for a quantum fluid [65], unless one is dealing either with liquid ^{4}He close to or below the lambda transition, or with liquid ^{3}He at $T<T_f$.

In the case of liquid parahydrogen, Reichman and Rabani [66] used a self-consistent quantum mode-coupling theory to derive, in the framework of the Kubo formalism and of the Gaussian approximation, a VACF for the dynamics of the molecular centers of mass, which is claimed to be reliable. On the other hand, recent quantum mechanical dynamic simulations (MCD) by Kinugawa [32], still carried out for the case of liquid parahydrogen, give also information on the same quantity, namely, the VACF. In this case, using the Gaussian approximation, we were able to obtain, in a preliminary work [62], a quite good agreement with the present experimental results at $T=14.3$ K (see Table I). Therefore in what follows we will assume the Gaussian approximation to be valid and, through it, we will try to extract all possible dynamic information from our experimental data on liquid parahydrogen measured on TOSCA. In practice, we will compare the experimental spectra taken on TOSCA (and processed as explained before) in order to obtain the experimental $S_{self}(k(\omega),\omega)$, with a theoretical model for the VACF, using the Gaussian approximation expressed by Eq. (22). We stress that the reason for the following detailed quantitative analysis is due to the good statistical accuracy of the present experimental spectra. However, we point out again that these are collected at constant scattering angle and therefore k changes with ω.

The basic ingredient of this comparison is in the definition of the *canonical* VACF according to the Kubo definition [see Eq. (25)]. Thus we define a normalized (time-symmetric) function $\Psi(t)$ as

$$\Psi(t)=\frac{u^c(t)}{u^c(0)}. \tag{30}$$

Using the results of the Kubo theory, it is easy to show that $u^c(0)=(3k_BT)/M$ and therefore,

$$u^c(t)=\frac{3k_BT}{M}\Psi(t). \tag{31}$$

The normalized correlation function $\Psi(t)$ is then assumed to obey a generalized Langevin equation (see Reichman and Rabani [66]), that is,

$$\dot{\Psi}(t)=-\int_0^t dt_1 K^c(t_1)\Psi(t-t_1), \tag{32}$$

where the dot means a time derivative and $K^c(t)$ is the memory function of the canonical VACF. The solution to Eq. (32) is easily obtained using the Laplace transform formalism. Actually, taking advantage of the time symmetry of $\Psi(t)$ and defining the two *real* spectral functions,

$$A(\omega)=\int_0^\infty dt\cos(\omega t)K^c(t), \tag{33}$$

$$B(\omega)=-\int_0^\infty dt\sin(\omega t)K^c(t), \tag{34}$$

we obtain the following expression for $\bar{\Psi}(\omega)$, the Fourier transform (FT) of $\Psi(t)$:

$$\bar{\Psi}(\omega)=\frac{1}{\pi}\frac{A(\omega)}{A^2(\omega)+[\omega+B(\omega)]^2}. \tag{35}$$

From the FT of Eq. (31), using also Eq. (26), we finally arrive at an expression for $J^c(\omega)$ and, from this, to a numerical evaluation of $J_A(\omega)$ and $J_S(\omega)$ [see Eqs. (27) and following]. These functions, in turn, can be used as input in Eq. (23) to obtain the *real* and *imaginary* parts of the squared displacement function $\gamma_1(t)$. From these, making use of Eqs. (22) and following, we obtain a numerical evaluation of the $S_{self}(k(\omega),\omega)$. This quantity can be compared with the experimental spectra.

In modeling the canonical memory function $K^c(t)$, we will begin considering the pair dynamics only. This is suggested by the relatively large values of the momentum transfer accessed by our experiment and, for the same reason, we do not expect our results to be much sensitive to the mode-coupling component of the canonical memory function. As a first attempt, we used a simple Gaussian model for $K^c(t)$. This is a good representation of the pair contribution to the memory function [2] and has been originally suggested by Singwi and Tosi (ST) [67]. Thus we define a canonical memory function of the form

$$K^c(t)=\Omega_0^2\exp[-(t/\tau_0)^2], \tag{36}$$

where Ω_0 is the Einstein frequency and τ_0 is a binary collision time [2].

A nonlinear fitting procedure was set up, using the mathematical machinery described in Sec. III, to obtain a VACF and then, through the Gaussian approximation, (see Sec. II and Ref. [39]) to work out the self inelastic structure factor, $S_{self}(k(\omega),\omega)$, along the TOSCA kinematic line $(k(\omega),\omega)$ to

TABLE II. Results of the fitting procedure of TOSCA experimental data making use of the Singwi-Tosi [67] model for the canonical memory function, including sample temperature T, reduced chi-squared data χ_r^2, Einstein frequency Ω_0, Gaussian binary collision time τ_0, and center-of-mass mean kinetic energy $\langle E_k \rangle$.

T (K)	χ_r^2	Ω_0 (meV)	τ_0 (ps)	$\langle E_k \rangle$ (K)
14.3(2)	6.27	8.01(9)	0.120(5)	63.6(4)
15.7(2)	3.34	7.95(9)	0.118(5)	63.5(4)
17.2(2)	3.56	7.87(9)	0.115(5)	63.5(4)
19.2(2)	1.35	7.68(9)	0.119(5)	63.4(4)
21.2(2)	0.656	7.40(9)	0.129(6)	63.1(4)

be compared with the experimental ones. The actual fitting procedure was implemented through a FORTRAN code making use of the MINUIT [68] standard minimizing routine. The spectrometer energy resolution was not included in the fit: experimentally estimated ($\Delta\hbar\omega = 0.43$ meV) at the energy transfer $\hbar\omega = 14.4$ meV from the solid parahydrogen measurements [55] was found totally negligible if compared to the typical width of the features of the liquid sample spectra. It is worth noticing that, after shifting the experimental data to get rid of the intramolecular $J=0 \rightarrow J'=1$ transition contribution (see Sec. IV), the aforementioned value of the energy resolution corresponded to $\hbar\omega = 0$ energy transfer. Experimental data were fitted in the energy interval (shifted) -10 meV $< \hbar\omega < 60$ meV and three parameters were obtained: an overall normalization constant, C, the Einstein frequency, Ω_0, and the Gaussian binary collision time, τ_0. Reduced χ^2 data and parameter estimates are reported in Table II for all the thermodynamic states.

Using Eqs. (16), (26), (27), and (31)–(35), the FORTRAN code was able to automatically evaluate the $f(\omega)$ and $g(\omega)$ spectral functions and, from the latter through Eq. (19), the center-of-mass mean kinetic energy, $\langle E_k \rangle$, which is also listed in Table II. Examples of the quality of the present fits are reported in Figs. 6(a) and 6(b) for parahydrogen liquid samples at $T=14.3$ K, and $T=19.2$ K, respectively. The agreement between experimental and simulated data is quite good in the whole energy interval (-10 meV$< \hbar\omega < 60$ meV), even though, reducing the sample temperature a negative trend in the fit quality becomes clearly visible (see also Table II): reduced χ^2 grows and exceeds 1.5 for the three lowest temperatures. In a second independent attempt, we used for the binary component of the canonical memory function an exponential model, according to a suggestion from Berne, Boon, and Rice (BBR) [69]. Thus we defined the following canonical memory function:

$$K^c(t) = \Omega_0^2 \exp(-t/\tau_1). \tag{37}$$

Here the reduced χ^2 turns out to be generally quite smaller than in the previous case but, again, the agreement between fits and experimental data worsens as the temperature decreases, as shown in Table III. New estimates of the Einstein frequency, Ω_0, of the exponential binary collision time, τ_1, and of the center-of-mass mean kinetic energy, $\langle E_k \rangle$, derived

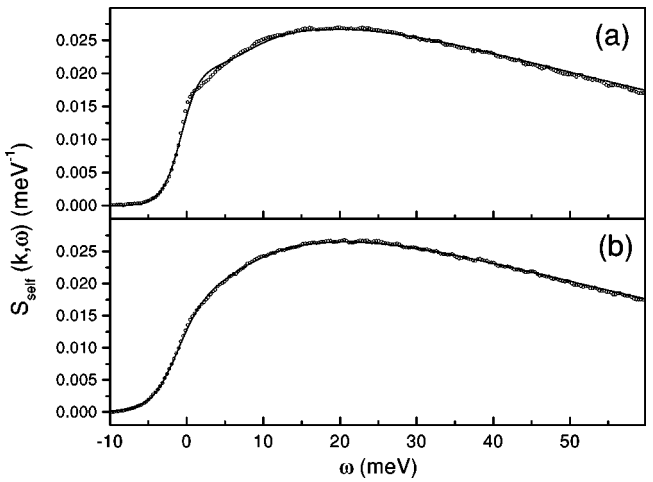

FIG. 6. Incoherent inelastic structure factor $S_{self}(k,\omega)$ measured along the TOSCA kinematic line (circles) and its Singwi-Tosi [67] best fit (solid line) for liquid parahydrogen at $T=14.3$ K (a), and $T=17.2$ K (b).

from the BBR fitting procedure are also reported in Table III for all the thermodynamic states.

A careful inspection of the two lowest temperature measurements ($T=14.3$ K and $T=15.7$ K) revealed that the disagreement between experimental data on one side, and ST and BBR fits on the other, was mainly confined in the energy interval -1 meV$< \hbar\omega < 13$ meV (see Fig. 7 for a zoom on $T=15.7$ K data), where the ST and BBR fitting functions exhibited an almost constant curvature, not at all followed by the experimental data. This suggested that some extra contribution in the $K^c(t)$ was necessary. Thus we attempted to fit the two lowest temperature spectra adding a long-time component to the canonical memory function. This long-time (mode-coupling) part was modeled using a recipe suggested by Levesque and Verlet [70] (LV) and we defined, accordingly, the following canonical memory function:

$$K^c(t) = \Omega_0^2 \exp[-(t/\tau_0)^2] + L t^4 \exp(-\alpha t). \tag{38}$$

Experimental data at $T=14.3$ K and $T=15.7$ K, unsatisfactory described by both ST and BBR models (see Tables II and III), were refitted using an LV canonical memory function in the energy interval (shifted) -10 meV$< \hbar\omega$

TABLE III. Results of the fitting procedure of TOSCA experimental data making use of the Berne-Boon-Rice [69] model for the canonical memory function, including sample temperature T, reduced chi-squared data χ_r^2, Einstein frequency Ω_0, exponential binary collision time τ_1, and center-of-mass mean kinetic energy $\langle E_k \rangle$.

T (K)	χ_r^2	Ω_0 (meV)	τ_1 (ps)	$\langle E_k \rangle$ (K)
14.3(2)	2.88	8.85(4)	0.099(2)	65.2(2)
15.7(2)	1.55	8.76(4)	0.099(2)	65.0(2)
17.2(2)	1.44	8.65(4)	0.098(2)	64.9(2)
19.2(2)	0.710	8.41(4)	0.103(2)	64.7(2)
21.2(2)	0.502	8.05(4)	0.116(3)	64.2(2)

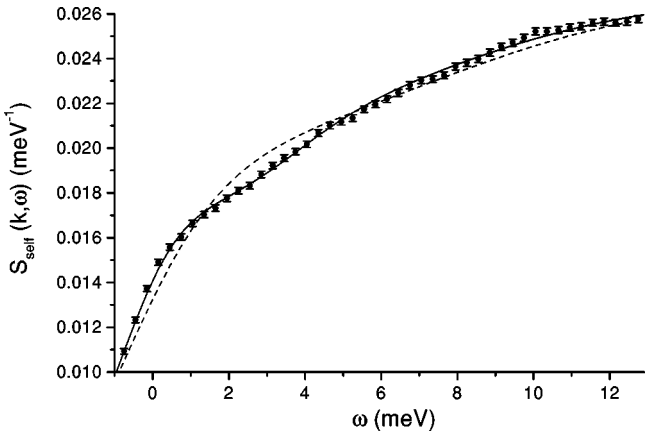

FIG. 7. Zoom on the incoherent inelastic structure factor $S_{self}(k,\omega)$ measured along the TOSCA kinematic line (circles with error bars), its Singwi-Tosi [67] best fit (dashed line), and its Levesque-Verlet [70] best fit (full line) for liquid parahydrogen at $T=15.7$ K.

<60 meV. Five parameters were obtained for each data set: an overall normalization constant, C, the Einstein frequency, Ω_0, the Gaussian binary collision time, τ_0, the long-time constant, L, and the long-time exponential decay, α. Reduced χ^2 values, LV fitting parameters and new $\langle E_k\rangle$ estimates are reported in Table IV for the two low-temperature thermodynamic states. It is evident that the reduced χ^2 now turns out to be much smaller than in the previous cases (see Tables II and III), but the LV fitting curve does not appear to be very sensitive to L and α, their uncertainties being quite large. An example of the good quality of the LV fits is reported in Fig. 7 for $T=15.7$ K data. However, the values of the parameters Ω_0 and τ_0 remain intermediate between the two previous (binary) cases. Therefore in the following we will limit the discussion to the pure binary models.

V. DISCUSSION AND CONCLUSIONS

The understanding of the fitting results reported in Tables II, III, and IV can be improved through a path integral Monte Carlo code, simulating the para-H_2 samples in the same thermodynamic conditions of the TOSCA experimental measurements (see Table I). These simulations were mainly carried out using the semiempirical isotropic pair potential derived by Silvera and Goldman [71] (SG), still considered one of the most reliable for para-H_2 in low-temperature condensed phases [72]. However, in order to test the effect of the potential on the simulated physical quantities (namely, $\langle E_k\rangle$ and Ω_0), one calculation (at $T=15.7$ K and $n=22.52$ nm^{-3}) was also performed using the more recent semiempirical isotropic pair potential derived by Norman, Watts, and Buck [73] (NWB). The main difference between the two is the presence in SG of a small repulsive term, C_9/r^9, which approximately takes into account the effect of the irreducible three-body interaction in the condensed phases. Generally, the PIMC algorithm was operated at one value, $P=64$, of the *Trotter number*, using $N=500$ classical particles [74]. However, at $T=15.7$ K and $n=22.52$ nm^{-3} a calculation using $P=81$ was also accomplished. Only tiny differences in the values of $\langle E_k\rangle$ and Ω_0, always smaller than 1%, were observed, both between the $P=64$ and $P=81$ results, and between SG and NWB ones. This check confirms that (a) the choice of the Trotter number $P=64$, is large enough to take into account correctly the quantum nature of the simulated systems and (b) the fine details of the potential do not play a crucial role in the evaluation of the two physical quantities of interest here. The PIMC code, already successfully employed for solid and liquid H_2 and liquid D_2 [55,75,74], makes use of the so-called *crude* estimator of the center-of-mass mean kinetic energy [22], while the Einstein frequency is evaluated, in the framework of isotropic pair interactions, through the quantum pair correlation function of the molecular centers of mass [2,5], $g(r)$,

$$\Omega_0^2=\frac{n}{3\hbar^2 M}\int d\vec{r}\,g(r)\nabla^2 V(r). \tag{39}$$

Here $V(r)$ is the intermolecular isotropic pair potential. Special care was taken in order to evaluate, and to correct for, the finite-size effects on Ω_0, caused by the cutoff of the $g(r)$ around $r=14$ Å. Details on the implementation of the PIMC code can be found in Ref. [74], while the results for $\langle E_k\rangle$ and Ω_0 are reported in Table V.

TABLE IV. Results of the fitting procedure of the two lowest-temperature TOSCA experimental data making use of the Levesque-Verlet [70] model for the canonical memory function, including sample temperature T, reduced chi-squared data χ_r^2, Einstein frequency Ω_0, Gaussian binary collision time τ_0, long-time constant L, long-time decay α, and the center-of-mass mean kinetic energy $\langle E_k\rangle$.

T (K)	χ_r^2	Ω_0 (meV)	τ_0 (ps)	L (meV^6)	α (meV)	$\langle E_k\rangle$ (K)
14.3(2)	1.114	8.25(8)	0.099(4)	$5(2)\times10^3$	7.0(6)	64.3(3)
15.7(2)	0.853	8.16(8)	0.098(4)	$7(2)\times10^3$	7.4(6)	64.2(3)

TABLE V. Estimates of the center-of-mass mean kinetic energy $\langle E_k\rangle$ and of the Einstein frequency Ω_0 obtained from quantum mechanical simulation procedures (namely, PIMC; see main text). The upper part of the table refers to the thermodynamic conditions of the experimental data. The lower part reports the PIMC results for the thermodynamic conditions of the parahydrogen simulations by Reichman and Rabani, and Kinugawa, respectively [66,32].

T(K)	n(nm^{-3})	$\langle E_k\rangle$ (K)	Ω_0 (meV)
14.3	22.91	61.4(1)	9.14(1)
15.7	22.52	61.4(1)	9.03(2)
17.2	22.10	61.3(1)	8.90(2)
19.2	21.50	61.6(1)	8.75(2)
21.2	20.83	62.0(1)	8.55(2)
14.0	23.50	63.2(1)	9.37(1)
14.7	24.18	66.8(1)	9.80(1)

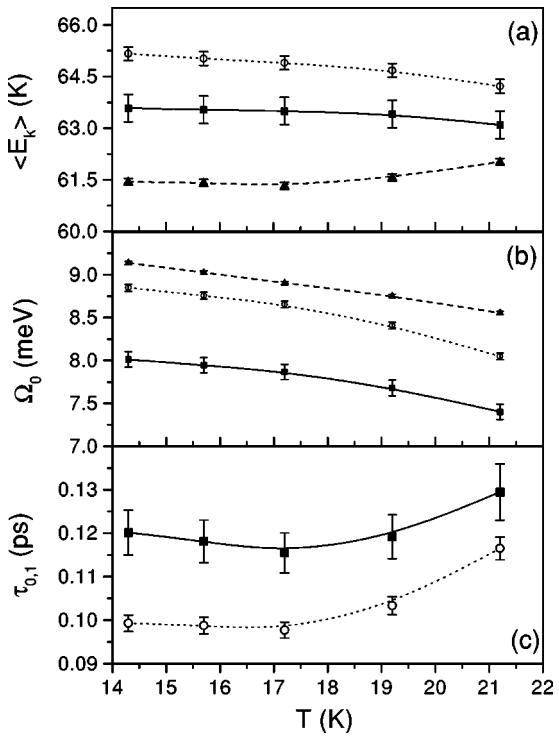

FIG. 8. Physical quantities estimated by fitting TOSCA experimental measurements (see Table I) making use of a Singwi-Tosi [see Eq. (36)] model for the canonical memory function (full squares) of a Berne-Boon-Rice [see Eq. (37)] model for the canonical memory function (open circles). Numerical values are reported in Tables II and III, respectively. Results from PIMC simulations (see also Table V) are shown as full triangles. Lines are data splines and are meant to be eye guides. Physical quantities stand for (a) center-of-mass mean kinetic energy $\langle E_k \rangle$; (b) Einstein frequency Ω_0; (c) Gaussian binary collision time, i.e., τ_0 for the Singwi-Tosi model, and exponential binary collision time τ_1 for the Berne-Boon-Rice one.

A comparison between the experimental estimates of the translational mean kinetic energy (both via ST and BBR) and the PIMC results is visible in Fig. 8(a). The two sets of fitted data follow a similar trend, but keep an almost constant offset of 1–1.5 K, corresponding to a relative discrepancy of about 1.5%. This discrepancy is larger than the respective statistical uncertainties, but the comparison with the typical relative accuracy of the results from the deep inelastic neutron scattering technique [55,75], i.e., 2–5 %, is quite satisfactory. The present results look promising even though PIMC data are included: although the fitting data cannot reproduce the slight peculiar trend of the simulated ones (given by the competition between decreasing density and growing temperature along the SVP line, e.g., in Table I), PIMC estimates of $\langle E_k \rangle$ lie close to the two sets of fitted data (ST and BBR), with a relative discrepancy of the order of 2.1% and 3.6%, respectively.

As far as the Einstein frequency is concerned, the experimental estimates (both from ST and BBR models) and the PIMC results are compared in Fig. 8(b). Here, the three sets of data exhibit a similar decreasing trend, which shows that the Einstein frequency, unlike the center-of-mass mean kinetic energy, is dominated almost exclusively by the density of the liquid. However, the relative discrepancy among the three different estimates is substantially larger than before: 6.6% between ST and BBR, 10.4% between ST and PIMC, and 3.8% between BBR and PIMC. These three sets of figures are clearly impossible to be reconciled among one another, given the statistical accuracy (always smaller than 1.1%, see also Tables II, III, and V). However, we should also note that the typical experimental method to evaluate Ω_0, making use of the measured pair correlation function in conjunction with Eq. (39), usually provides values with a comparable accurateness (around 10–12%), in the case of liquid ^{4}He [76].

The third physical quantity evaluated through the fitting procedure, namely, the binary collision times, τ_0 (from ST) and τ_1 (from BBR), cannot be easily obtained from an equilibrium simulations like PIMC. Actually some approximate expressions exist [2] but they appear justified only in a classical framework, rather inappropriate in our case. For this reason, we decided to report in the figure only the fit results from the two canonical memory function models in Fig. 8(c). The two sets of data, τ_0 and τ_1, show a similar trend even though they exhibit an overall discrepancy of the order of 9%. This figure looks quite large but we should also observe that the two physical quantities are not equivalent. In fact, both τ represent the value of t at which $K^c(t)/K^c(0)=1/e$, but the shape of the two canonical memory functions is very different, and so are the properties of the VACF they generate. For example, the fourth moment of the $f(\omega)$ obtained through the BBR approach is infinite, i.e., physically incorrect.

While the comparison at the level of the translational mean kinetic energy is quantitatively satisfactory and that for the Einstein frequency is still acceptable, the same picture does not hold for more involved dynamic quantities. For example, it is interesting to compare the spectral function $f(\omega)$, which is obtained from the present fitting procedures, and two independent theoretical derivations of the same quantity. The first is obtained from a MCD quantum mechanical dynamic simulation [32], and the second from a QMC calculation [66]. The simulated spectral functions $f(\omega)$ have been derived from the published spectral functions $J(\omega)$ as explained in Sec. II and then properly normalized. The comparison at the level of $\langle E_k \rangle$ and Ω_0 is easily obtained relating the results in Tables II and III with the same quantities reported in Table V, and shows a fair agreement. However, when the same comparison is extended to the spectral function $f(\omega)$, substantial differences become apparent. This is shown in Fig. 9(a). In the following we will discuss more accurately about the aforementioned quantities, starting from $\langle E_k \rangle$ and Ω_0.

The fit results and their PIMC simulations have been already discussed in this section and are reported in Tables II, III, and V. For MCD and QMC, from the appropriate $f(\omega)$ spectral moments, one obtains $\langle E_k \rangle = 64.8$ K, $\Omega_0 = 8.35$ meV, and $\langle E_k \rangle = 63.8$ K, $\Omega_0 = 9.34$ meV, respectively, while our PIMC results for their corresponding thermodynamic conditions are in the same order: $\langle E_k \rangle = 66.8(1)$ K, $\Omega_0 = 9.80(1)$ meV, and $\langle E_k \rangle$

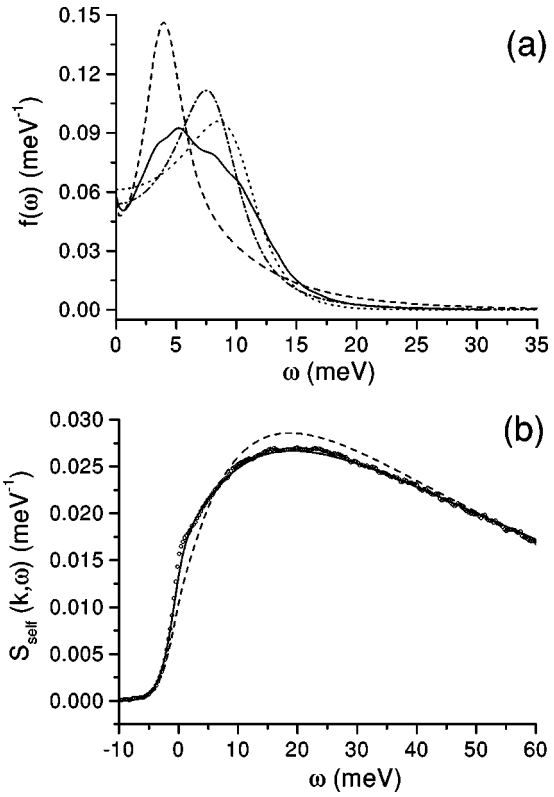

FIG. 9. (a) Comparison among liquid p-H_2 spectral functions $f(\omega)$ obtained from a molecular centroid dynamics simulation [32] at $T=14.7$ K (solid line), from the quantum mode-coupling [66] approach at $T=14.0$ K (dashed line), from a Singwi-Tosi [see Eq. (36)] fit of the experimental data at $T=14.3$ K (dotted line), and from a Berne-Boon-Rice [see Eq. (36)] fit of the same data set (dotted-dashed line). (b) Incoherent inelastic structure factor of liquid p-H_2 calculated along the TOSCA kinematic path and derived from the two simulated spectral functions $f(\omega)$ shown in panel (a) (namely, MCD, full line, and QMC, dashed line) together with the experimental data at $T=14.3$ K (circles).

$=63.2(1)$ K, $\Omega_0=9.37(1)$ meV (see also Table V). It is worth noting that despite the lack of information about simulated data statistical precision, the agreement on the center-of-mass mean kinetic energy between PIMC and dynamic calculations looks reasonably good for both MCD and QMC, while the PIMC value of the Einstein frequency is better reproduced by QMC than by MCD. This fact, which resembles the behavior of the fitted values of Ω_0 in Tables II and III, is not totally surprising since the QMC method makes extensive use of the results of equilibrium PIMC simulations [43,66], performed, by the way, through the same isotropic pair potential [71] we used in ours. On the other hand, the skewness and the peakness of the four curves appear immediately all different. In this respect, it is very useful to compare the values of binary collision time, which is connected to the fourth moment of $f(\omega)$ by [5]

$$\int_{-\infty}^{+\infty} \omega^4 f(\omega) d\omega = \Omega_0^2(\Omega_0^2 + 2\tau_0^{-2}). \tag{40}$$

From the two dynamic simulations we obtain: $\tau_0 = 0.0441$ ps for QMC and $\tau_0 = 0.0928$ ps for MCD. The discrepancy among MCD, QMC, and fitted values of the binary collision time [$\tau_0 = 0.120(5)$ ps at $T=14.3$ K using the ST model memory function] is in this case quite large: the ST estimate of τ_0 is almost three times larger than the QMC value and the MCD τ is, in turn, more than twice larger than the QMC one. Transformed from energy into time domain, this means that what is not equally described should be the intermediate- and long-time velocity autocorrelation function behavior. Actually the infinite-time limit of the self-dynamics [epitomized by the self-diffusion coefficient, D] seems almost satisfactorily reproduced in Fig. 9(a) by all the spectral functions [D being proportional to $f(\omega=0)$], so we might infer that is the intermediate-time behavior of the VACF to be still lacking precision, from the experimental, the analytical, and the simulation points of view. By hindsight, it is not entirely surprising that the moments predicted by QMC are reasonable because these moments are used as the input for mode-coupling calculations. The original mode-coupling idea was introduced [77] to interpret long-time tails but did not quantitatively reproduce the intermediate regime of VACF [2]. For the same reason, QMC results also may exhibits problems in the intermediate regime of the correlation function. In contrast, MCD results should be more reliable in this regime.

An alternative explanation is the possible failure, in our (k,ω) range, of the Gaussian approximation [defined in Eq. (22)], which is used both in the experimental data analysis and in the QMC approach [66], but not by MCD. However, since this approximation is applied in rather different ways (as a fit in the present work, iteratively by QMC), fitted and QMC results could diverge towards different and unpredictable directions: this fact would be sufficient to explain why the three methods, namely, experimental, QMC, and MCD, exhibit the aforementioned discrepancies. Of course, this makes very important a precise check of the validity of the Gaussian approximation and its range of applicability.

The comparison between QMC and MCD simulations results, coupled with the Gaussian approximation of Eq. (22) to obtain $S_{self}(k(\omega),\omega)$, and experimental data at $T=14.3$ K is finally summarized in Fig. 9(b). It is evident that the MCD self inelastic structure factor (reduced $\chi^2=5.565$) is much more similar to TOSCA data than the QMC one (reduced $\chi^2=90.78$), despite the thermodynamic conditions of the latter being closer to the experimental density and temperature (see Table V). Since the Gaussian approximation has been used in the QMC case not only by us to produce $S_{self}(k(\omega),\omega)$ from $f(\omega)$, but also, in a self-consistent way, to obtain the QMC $f(\omega)$ itself, we have to conclude that QMC results are impossible to be reconciled with our experimental findings [i.e., our $S_{self}(k(\omega),\omega)$]. However, we still cannot decide, provided our experimental data are faultless, whether this problem is caused by the failure of the Gaussian approximation or by some other assumptions in the QMC routines used. On the contrary, MCD did not make use of this approximation to work out its $f(\omega)$.

In conclusion, in the present study we have recorded the incoherent inelastic neutron cross section of liquid and solid parahydrogen in various thermodynamic conditions using the

neutron spectrometer TOSCA. The measured cross section provided direct experimental access to the incoherent part of the inelastic structure factor for the centers of mass of the H_2 molecules in the system under observation. Measured data have been corrected for the experimental effects and then processed in the framework of the Young-Koppel model in order to remove the contributions coming from the intramolecular (rotovibrational) dynamics. The Gaussian approximation has been then assumed, aiming to relate the incoherent scattering law of the liquid samples to the energy spectrum of their velocity autocorrelation functions. These correlation functions have been subsequently obtained from a fitting procedure, making use of the quantum generalized Langevin equation and two model memory functions, namely, with a Gaussian and an exponential time decay. The fitted energy spectra of the velocity autocorrelation function have been also compared to the most recent results of both centroid molecular dynamics and self-consistent quantum mode-coupling theory. Three moments of the energy spectrum of the velocity autocorrelation function were related to important physical quantities (namely, center-of-mass mean kinetic energy, Einstein frequency, and binary collision time) and the first two were also simulated through a standard (equilibrium) path integral Monte Carlo code. The results of this comparison came out very interesting and, for example, showed that the center-of-mass mean kinetic energy and the Einstein frequency can be experimentally evaluated using this fitting procedure with a similar (or even better) level of accuracy than what is normally achieved by more usual experimental techniques. However, the analysis of the binary collision time and a careful review of the experimental and simulated energy spectra of the velocity autocorrelation function showed that large inconsistencies still exist both between experimental and simulated data and between simulated data from the two different approaches. Summarizing, we conclude that further development of theoretical and simulation approaches, as well as more extensive experimental efforts, are necessary. In addition, a comprehensive check of the validity of the Gaussian approximation in liquid H_2 is also highly needed.

ACKNOWLEDGMENTS

The superb technical assistance of the ISIS Instrument Division (Rutherford Appleton Laboratory, Chilton, Didcot, UK) is gratefully acknowledged. The authors are greatly indebted to Dr. U. Bafile (CNR-IFAC, Firenze, Italy) for invaluable comments on the present work. One of the authors (D.C.) is also indebted to Dr. S. F. Parker and Dr. J. Tomkinson (ISIS, Rutherford Appleton Laboratory, Chilton, Didcot, UK) for the encouragement and many useful and stimulating discussions on the subject of this paper.

[1] See, for example, J. Phys.: Condens. Matter **12**, (8A) (2000), special issue for the 4th EPS liquid matter conference, edited by P. Tarazona, L. Reatto, and R. Hidalgo-Alvarez.
[2] U. Balucani and M. Zoppi, *Dynamics of the Liquid State* (Oxford University Press, Oxford, 1994).
[3] M. P. Allen and D. J. Tildesley, *Computer Simulation of Liquids* (Oxford University Press, Oxford, 1987).
[4] See, for example, S. Moroni, D. E. Galli, S. Fantoni, and L. Reatto, Phys. Rev. B **58**, 909 (1998), and references therein.
[5] S. W. Lovesey, *Theory of Neutron Scattering from Condensed Matter* (Oxford University Press, Oxford, 1987), Vol. I.
[6] P. A. Egelstaff, *Liquid State* (Clarendon Press, Oxford, 1992).
[7] L. Van Hove, Phys. Rev. **95**, 249 (1954).
[8] H. R. Glyde, *Excitations in Liquid and Solid Helium* (Clarendon Press, Oxford, 1994).
[9] C. G. Windsor, *Pulsed Neutron Scattering* (Taylor and Francis, London, 1981).
[10] A. M. Dyugaev, J. Low Temp. Phys. **78**, 79 (1990).
[11] F. Barocchi, M. Neumann, and M. Zoppi, Phys. Rev. A **36**, 2440 (1987).
[12] N. Metropolis, A. W. Rosenbluth, M. N. Rosenbluth, A. H. Teller, and E. Teller, J. Chem. Phys. **21**, 1087 (1953).
[13] J. P. Hansen and I. R. McDonald, *Theory of Simple Liquids* (Academic, London, 1986).
[14] B. J. Alder and T. E. Wainwright, J. Chem. Phys. **31**, 459 (1959).
[15] A. Rahman, Phys. Rev. **136**, A405 (1964).
[16] L. Verlet, Phys. Rev. **159**, 98 (1967).
[17] *Molecular Dynamics Simulation of Statistical-Mechanical Systems*, edited by G. Ciccotti and W. G. Hoover (North-Holland, Amsterdam, 1986).
[18] J. A. Barker, J. Chem. Phys. **70**, 2914 (1979).
[19] E. L. Pollock and D. M. Ceperley, Phys. Rev. B **30**, 2555 (1984).
[20] B. J. Berne and D. Thirumalai, Annu. Rev. Phys. Chem. **37**, 401 (1986).
[21] D. M. Ceperley and E. L. Pollock, Phys. Rev. Lett. **56**, 351 (1986).
[22] D. M. Ceperley, Rev. Mod. Phys. **67**, 279 (1995).
[23] R. P. Feynman and A. R. Hibbs, *Quantum Mechanics and Path Integrals* (McGraw-Hill, New York, 1965).
[24] R. P. Feynman, *Statistical Mechanics* (Benjamin, Reading, MA, 1972).
[25] H. F. Trotter, Proc. Am. Math. Soc. **10**, 545 (1959).
[26] D. Chandler and P. G. Wolynes, J. Chem. Phys. **74**, 4078 (1981).
[27] J. Cao and G. A. Voth, J. Chem. Phys. **100**, 5093 (1994); **100**, 5106 (1994); **101**, 6157 (1994); **101**, 6168 (1994); **101**, 6184 (1994).
[28] G. J. Martyna, J. Chem. Phys. **104**, 2018 (1996).
[29] J. Cao and G. J. Martyna, J. Chem. Phys. **104**, 2028 (1996).
[30] M. Pavese and G. A. Voth, Chem. Phys. Lett. **249**, 231 (1996).
[31] A. Calhoun, M. Pavese, and G. A. Voth, Chem. Phys. Lett. **262**, 415 (1996).
[32] K. Kinugawa, Chem. Phys. Lett. **292**, 454 (1998).
[33] G. Ciccotti, C. Pierleoni, F. Capuani, and V. S. Filinov, Chem. Phys. Lett. **121-122**, 452 (1999).
[34] P. Nozières and D. Pines, *Theory of Quantum Liquids, Vol. II:*

Superfluid Bose Liquids (Addison-Wesley, Redwood City, CA, 1990).
[35] *Momentum Distribution*, edited by R. N. Silver and P. E. Sokol (Plenum, New York, 1989).
[36] K. W. Herwig, P. E. Sokol, T. R. Sosnick, W. M. Snow, and R. C. Blasdell, Phys. Rev. B **41**, 103 (1990).
[37] M. Celli, M. Zoppi, and J. Mayers, Phys. Rev. B **58**, 242 (1998).
[38] G. H. Vineyard, Phys. Rev. **110**, 999 (1958).
[39] A. Rahman, K. S. Singwi, and A. Sjölander, Phys. Rev. **126**, 986 (1962).
[40] M. Nelkin and A. Ghatak, Phys. Rev. **135**, A4 (1964).
[41] R. Zwanzig, Phys. Rev. **133**, A50 (1964).
[42] V. F. Sears, Proc. Phys. Soc. London **86**, 953 (1965).
[43] E. Rabani and D. R. Reichman, Phys. Rev. E **65**, 031203 (2002).
[44] R. Zwanzig, *Lectures in Theoretical Physics* (Wiley, New York, 1961), Vol. III.
[45] H. Mori, Prog. Theor. Phys. **33**, 423 (1965).
[46] H. Mori, Prog. Theor. Phys. **34**, 399 (1965).
[47] R. Kubo, M. Toda, and N. Hashitsume, *Statistical Physics II, Solid State Science*, 2nd ed. (Springer, Berlin, 1995).
[48] S. W. Lovesey, J. Phys. C **6**, 1856 (1973).
[49] F. J. Bermejo, B. Fäk, S. M. Bennington, R. Fernandez-Perea, C. Cabrillo, J. Dawidowski, M. T. Fernandez-Diaz, and P. Verkerk, Phys. Rev. B **60**, 15 154 (1999).
[50] F. J. Bermejo, K. Kinugawa, C. Cabrillo, S. M. Bennington, B. Fäk, M. T. Fernandez-Diaz, P. Verkerk, J. Dawidowski, and R. Fernandez-Perea, Phys. Rev. Lett. **84**, 5359 (2000).
[51] F. Barocchi, M. Moraldi, and M. Zoppi, Phys. Rev. A **26**, 2168 (1982).
[52] R. Kubo, Rep. Prog. Phys. **29**, 255 (1966).
[53] Z. A. Bowden, M. Celli, F. Cilloco, D. Colognesi, R. J. Newport, S. F. Parker, F. P. Ricci, V. Rossi-Albertini, F. Sacchetti, J. Tomkinson, and M. Zoppi, Physica B **276-278**, 98 (2000).
[54] M. Zoppi, L. Ulivi, M. Santoro, M. Moraldi, and F. Barocchi, Phys. Rev. A **53**, R1935 (1996).
[55] M. Celli, D. Colognesi, and M. Zoppi, Eur. Phys. J. B **14**, 239 (2000).
[56] J. A. Young and J. U. Koppel, Phys. Rev. A **135**, 603 (1964).
[57] A. Bickermann, H. Spitzer, H. Stiller, H. Meyer, R. E. Lechner, and F. Volino, Z. Phys. B **31**, 345 (1978).
[58] M. Zoppi, Physica B **183**, 235 (1993).
[59] R. D. McCarty, J. Hord, and H. M. Roder, NBS Monogr. **168**, 6-1 (1981).
[60] K. Carneiro, Phys. Rev. A **14**, 517 (1976).
[61] A. K. Agrawal, Phys. Rev. A **4**, 1560 (1971).
[62] M. Zoppi, D. Colognesi, and M. Celli, Europhys. Lett. **53**, 34 (2001).
[63] D. E. O'Reilly and E. M. Peterson, J. Chem. Phys. **66**, 934 (1977).
[64] M. Celli, N. Rhodes, A. K. Soper, and M. Zoppi, J. Phys.: Condens. Matter **11**, 10 229 (1999).
[65] M. Neumann and M. Zoppi, Phys. Rev. E **65**, 031203 (2002).
[66] D. R. Reichman and E. Rabani, Phys. Rev. Lett. **87**, 265702 (2001).
[67] K. S. Singwi and M. P. Tosi, Phys. Rev. **157**, 153 (1967).
[68] F. James, *MINUIT Minimization Package: Reference Manual* (CERN Program Library, Geneva, 1994).
[69] B. J. Berne, J. P. Boon, and S. A. Rice, J. Chem. Phys. **45**, 1086 (1966).
[70] D. Levesque and L. Verlet, Phys. Rev. A **2**, 2514 (1970).
[71] I. F. Silvera and V. V. Goldman, J. Chem. Phys. **69**, 4209 (1978).
[72] Q. Wang, J. K. Johnson, and J. Q. Broughton, Mol. Phys. **89**, 1105 (1996).
[73] M. J. Norman, R. O. Watts, and U. Buck, J. Chem. Phys. **81**, 3500 (1984).
[74] M. Neumann and M. Zoppi, Phys. Rev. A **40**, 4572 (1989); M. Zoppi and M. Neumann, Phys. Rev. B **43**, 10 242 (1991).
[75] M. Zoppi, D. Colognesi, and M Celli, Eur. Phys. J. B **23**, 171 (2001).
[76] V. F. Sears, Phys. Rev. B **28**, 5109 (1983).
[77] W. Götze and M. Lücke, Phys. Rev. B **13**, 3822 (1976); **13**, 3825 (1976).